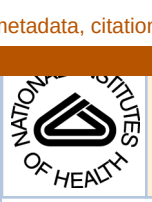

Published in final edited form as:

Adv Mater. 2012 June 12; 24(22): 2992–2998. doi:10.1002/adma.201200706.

Hybrid 2D Nanomaterials as Dual-mode Contrast Agents in Cellular Imaging

Tharangattu N. Narayanan[1], **Bipin K. Gupta**[2], **Sajna A. Vithayathil**[3], **Rebeca R. Aburto**[1,4], **Prof. Sendurai A. Mani**[3], **Jaime Taha-Tijerina**[1], **Bin Xie**[5], **Benny A. Kaipparettu**[4], **Suzy V. Torti**[5], and **Prof. Pulickel M. Ajayan**[1]

Pulickel M. Ajayan: ajayan@rice.edu

[1]Department of Mechanical Engineering and Materials Science, Rice University, 6100 Main Street, Houston, TX 77006, USA

[2]National Physical Laboratory (CSIR), Dr. K. S. Krishnan Road, New Delhi 110012, India

[3]Department of Molecular and Human Genetics, Dan L. Duncan Cancer Center, Baylor College of Medicine, Houston, TX 77030, USA

[4]Department of Molecular Pathology, MD Anderson Cancer Center, 7435 Fannin Street, Unit # 951, Houston, TX 77054, USA

[5]Department of Biochemistry, Wake Forest School of Medicine, Winston-Salem, NC 27157, USA

Keywords

hybrid materials; imaging techniques; magnetic resonance imaging; luminescence; graphene oxide

The design of multifunctional nanofluids is highly desirable for biomedical therapy/cellular imaging applications.[1–4] The emergence of hybrid nanomaterials with specific properties, such as magnetism and fluorescence, can lead to an understanding of biological processes at the biomolecular level.[1] Various hybrid systems have been analyzed in the recent past for several possible biomedical applications.[5–9] Carbon-based hybrid systems such as carbon nanotubes with various nanoparticles are being widely tested for their biological applications because of their ability to cross cell membranes and their interesting thermal and electrical properties.[10,11] Graphene oxide (GO) is a fairly new graphene-based system with a 2D carbon honeycomb lattice decorated with numerous functional groups attached to the backbone: these functional groups make it an excellent platform for further attachment of nanoparticles and synthesis of hybrid materials. Cell viability studies on GO have been recently attempted, showing biocompatibility. [12,13] Moreover, the intrinsic photoluminescence (PL) properties of GO can be utilized for cellular imaging.[13] The large surface area and non-covalent interactions with aromatic molecules make GO an excellent system for biomolecular applications and drug attachment.

On the other hand, magnetic-field-assisted biomolecular imaging, drug delivery, and therapy have received tremendous attention in nano-biotechnology since the proposal of magnetic materials for hyperthermia treatment of cancer, in 1957.[14] Iron oxide (Fe_3O_4) occupies a unique position among the various magnetic materials as a result of its considerable saturation magnetization (87 emu g^{-1}), interesting transport properties, and, above all, high

*Correspondence to: Prof. P. M. Ajayan (ajayan@rice.edu).

Supporting Information

Supporting Information is available from the Wiley Online Library or from the author.

bio-compatibility.[2] Aqueous ferrofluids based on superparamagnetic iron oxide (SPION, ultrafine Fe_3O_4 nanoparticles having size ~10 nm) are well proven for their biomedical applications such as magnetic hyperthermia (using their radio-frequency power loss), magnetic contrast enhancement, enzyme immobilization, and drug targeting and delivery. [10]

The advent of state-of-the-art biomedical imaging tools has helped the development of cell imaging/tracking or gene monitoring with high temporal and spatial resolution.[15,16] Non-invasive multimodality techniques are also rapidly changing the evolving field of experimental imaging based on genetic expression and thus becoming suitable for future clinical practice. Each imaging technique has its own limitations, and multimodality imaging agents can address this hurdle. Magnetic resonance imaging (MRI) is an important diagnostic tool and is unique in its ability to generate 3D images of opaque and soft tissues with high spatial resolution. More interestingly, contrast in MR images arising from the variation in inherent relaxation times can be manipulated using contrast agents. But, despite its competitive molecular imaging capability, the inherent low sensitivity of the MRI technique demands the synthesis of high contrast enhancement agents. This has led to the use of nanoparticles of gadolinium (Gd, paramagnetic) and iron oxide (ferromagnetic/ superparamagnetic) as high relaxivity contrast enhancement agents.

Hybrid materials can also enable non-invasive imaging methods and diagnosis protocols by combining the unique properties of the individual system. Advances in nanotechnology have led to the development of hybrid versions of these nanoparticles, which can improve upon the low sensitivity of MRI by other techniques such as fluorescence. Fluorescence allows bio-imaging with high speed and sensitivity. It has been established that a combination of magnetic and fluorescent imaging techniques with nanostructured systems will be beneficial for in vivo disease diagnosis and in vitro monitoring of living cells.[17] However, the synthesis of highly luminescent biomaterials using ferromagnetic/superparamagnetic Fe_3O_4 is a complicated development owing to the fluorescence quenching property of Fe_3O_4. Researchers have developed lumino-magnetic phosphors for cell imaging applications, [18] but all those nanophosphor materials are paramagnetic in nature, limiting their bio-applications with low magnetic field assistance. Such a multimodality technique can combine the high spatial (50 μm) and temporal resolution of MRI with the high sensitivity of optical imaging probes, and most MRI/optical multimodal agents are based on organic dyes.[1] Though SPIONs have been commercially identified for their applications in T2-weighted MRI contrast enhancement, other imaging modalities using bare SPIONs cannot be realized. Recently, core/shell nanoparticles with SPIONs and polymer-passivated SPION/ metallic hybrid structures have proven their efficacy in other modalities such as optical imaging, magnetomotive photoacoustic imaging, and scattering-based imaging.[19–21]

Here we report the synthesis and demonstration of a single hybrid nanosystem for dual-mode cellular imaging using PL and MRI. An aqueous suspension of 2D nanofillers of GO-Fe_3O_4 (GO-F) at neutral pH (~7) is synthesized by a simple chemical route. Recently, there have been some reports on the synthesis of iron oxide functionalized GO particles by different chemical routes,[22–24] but the material has not been exploited in bio-imaging applications. Here we discuss a detailed PL study conducted on this nanofluid and its in vitro cancer cell imaging, hence demonstrating GO-F as a possible multimodalagent without any cell cytotoxicity. Direct use of iron oxide ($Fe_3O_4/\gamma Fe_2O_3$) for targeted drug delivery is not efficient owing to a “drug burst” effect (quick release of the drug upon injection) before the desired site is reached, and GO-F may be a better candidate since it has been demonstrated using Rhodamine molecules that aromatic drug molecules can be directly attached to the GO lattice. [25–27] In addition, theoretical evaluation of radio frequency power loss by measuring the specific absorption rate (SAR) for Fe_3O_4 nanoparticles having

size ~10 nm shows high values, indicating their suitability for applications in magnetic hyperthermia.[28] However, the heat transfer ability of Fe_3O_4-based ferrofluid is comparatively poor. The high heat transfer ability/thermal conductivity of GO can make GO-F an ideal material for hyperthermia applications.

Development of a GO-SPION-based hybrid system will also help in the investigation of the role of different parameters, such as surface roughness, functional groups, and shape/morphology of nanoparticles, in creating bio/nano interfaces.[29–31] Mahmoudi and Serpooshan proved that SPIONs with jagged surfaces can absorb various biomolecules/proteins much more strongly than SPIONs with smooth surfaces.[29] The GO flake platform also has considerable surface roughness and contains many functional groups, making it a unique material for understanding the biophysical properties at bio/nano interfaces.

We studied nanofluid stability using zeta potential measurements (Malvern Zen 3600 Zetasizer) along with measurements of the hydrodynamic radius of the particles by dynamic light scattering. The zeta potential of GO-F is −48.7 mV, indicating “good stability” of the nanofluid. This guarantees a long shelf-life. The hydrodynamic radius of GO-F was found to be ~583 nm. In situ chemical synthesis allows Fe_3O_4 nanoparticles to be covalently attached on to the GO surface.[16] Hence, the GO-F stable suspension is formed through the oxygen functionalities of GO with Fe_3O_4. Small flakes of GO, after sonication for 3 h, were fully suspended in water for 2 days. A schematic of GO-F is shown in Figure 1a. Epoxy, carboxyl, or hydroxyl groups available in GO make it chemically bond with Fe_3O_4. This was further verified by Fourier transform infrared (FTIR) analysis.

A TEM image of GO-F is shown in Figure 1b. The Fe_3O_4 nanoparticles having a size of approximately 10 nm are uniformly distributed in GO. High-resolution TEM (HRTEM) images and a selected area electron diffraction (SAED) image showing the (311) lattice plane of Fe_3O_4 (with dark contrast) are shown in the Supporting Information (Figure S1). In order to prove the graphitic nature of the nanocomposite sample, micro-Raman studies were conducted with GO-F powder; the result is shown in Figure 1c. Graphitic G (order) and D (disorder) Raman modes are marked in the figure. The higher intensity G peak indicates the extent of graphitization of the sample. The inset in this figure is a photograph of a stable GO-F suspension. The magnetic nature of the powder was verified using a vibrating sample magnetometer (VSM). The room temperature (300 K) magnetization $M(H)$ curve is depicted in Figure 1d. The sample shows a typical superparamagnetic S-like curve, which indicates the contribution of ultrafine Fe_3O_4. The XRD pattern of the GO-F powder is shown in Figure 1e. It consists of broad amorphous-like peaks around 24° and 44°, corresponding to GO having a lattice spacing of ~0.39 nm. The XRD results also indicate the presence of Fe_3O_4 (International Centre for Diffraction Data, ICDD: 750449). FTIR spectra of GO and GO-F are shown in Figure 1f. The presence of different types of oxygen functionalities in GO is evident from peaks corresponding to oxygen stretching vibration (2900–3600 cm^{-1}, –OH vibration), C=O stretching vibration (1720 cm^{-1}), C–OH stretching vibration (1220 cm^{-1}), and C–O stretching vibration (1060 cm^{-1}) in Figure 1f (dark line). Moreover, the signature of aromatic C=C stretching at ~1600 cm^{-1} indicates the presence of the sp^2 hybridized honeycomb lattice. The GO-F also contains these functional groups, but the positions of the bonds are red shifted and the sharpness of the peaks is changed, particularly that of aromatic C=C bonding (Figure 1e; light line). This indicates the change in the coordination environment of various functional groups in GO-F. Peaks between 400 and 700 cm^{-1} correspond to those of Fe-O in Fe_3O_4. The shift in the peak position and modification of C=C bonding is proposed as evidence for covalent bonding in GO with other nanoparticles. The presence of iron oxide in GO-F is further understood from the XPS analysis. The Fe 2p XPS spectrum of GO-F is shown in Figure 1f (the complete XPS spectrum is provided in Figure S2 in the Supporting Information). The peaks of Fe 2p1/2

and Fe 2p3/2 at 710.9 eV and 725 eV, respectively, establish the fact that the iron oxide in the sample is Fe_3O_4. To explore the facets of chemical interactions, interfacial effect, and associated optical properties of GO-F nanofluid, we characterized the pristine GO, Fe_3O_4 ferrofluid, and GO-F suspensions (in water) through UV-visible absorption spectroscopy. Figure 2a shows the absorption spectra of Fe_3O_4, GO, and GO-F. The absorption result reveals that GO-F is optically transparent in the 700–800 nm range. A blue shift of the absorption edge is noticed when the absorption spectrum of GO-F is compared to that of Fe_3O_4 ferrofluid. A higher concentration of Fe_3O_4 nanoparticles in GO strengthens such effects and therefore leads to the blue shift of the absorption spectrum. The blue shift of the absorption edge for GO-F can be attributed to two factors: a) the integration effect in the bandgap due to composite formation between GO (1.70 eV)[32] and Fe_3O_4 (~2.9 eV), [33] and b) the surface interaction and interface formation effect between Fe_3O_4 and functional groups present in GO.[34,35] The absorption peak at ~250 nm throws light onto the fact that a strong interface has formed between GO and Fe_3O_4 (since the absorption peaks of pristine GO and Fe_3O_4 are observed at ~228 nm and ~354 nm, respectively). This has been further confirmed by PL spectroscopy.

Figure 2b exhibits the PL emission spectrum of Fe_3O_4 ferrofluid. An emission peak is observed at 416 nm upon excitation at 365 nm wavelength(3.39 eV) and Figure 2c represents the corresponding PLE (excitation) spectrum for Fe_3O_4 nanoparticles at 416 nm (2.98 eV) emission of Fe_3O_4 nanoparticles. The observed result is consistent with other reports.[36] To investigate further the chemical interaction and the interface formation between GO and Fe_3O_4, rigorous PL studies on the GO-F hybrid system were performed. PL results are shown in Figures 2d–f. In order to confirm the interface formation, we excited the hybrid system at 365 nm wavelength, which will help to make a comparative study with Fe_3O_4. Interestingly, the PL emission spectrum of the GO-F hybrid system shows two strong peaks. One of them can be attributed to Fe_3O_4 and the other to the interface formation between GO and Fe_3O_4, as expected, through oxygen functionalities. In order to ensure that the extra peak represents the interface formation, we performed a PLE experiment. This will compute the actual excitation of the GO-F hybrid system. Figure 2e is the PLE spectrum of GO-F at 469 nm emission. Figure 2f shows strong blue peak emission centered at 469 nm with estimated color coordinates $x = 0.2035$, $y = 0.2427$ of the GO-F nanocomposite at 324 nm excitation wavelength. Moreover, we also performed PL emission spectroscopy of the pristine GO sample at 324 nm excitation to ensure that the additional peak is due to interface formation (Figure 2h). The enhanced luminescence in GO-F arises from the interface between GO and Fe_3O_4 nanoparticles through oxygen functionalities, that is, carboxyl, carbonyl, epoxy, and hydroxyl groups, present in GO nanoparticles. A strong blue emission of the hybrid is ascribed to the integration of surface effects of GO-F and optical emission of Fe_3O_4 nanoparticles.

To know the efficacy of the GO-F nanofluid system as an efficient fluorescent marker, we performed time-resolved photoluminescence (TRPL)spectroscopy. Luminescence decay profiles of GO-F are shown in Figure 2i. Decay was recorded for the GO-F transitions at 469 nm for emission at 371 nm excitation measured at room temperature by a time-correlated single photon counting technique. Lifetime data of the GO-F hybrid were very well fitted to a double-exponential function as shown in Figure 2i. Parameters generated from iterative reconvolution of the decay with the instrument response function (IRF) are listed in Figure 2j. Observed lifetimes of the GO-F are $\tau_1 = 0.70$ ns and $\tau_2 = 4.80$ ns. For double-exponential decay, the average lifetime, τ_{av}, is determined by[15,37,38]

$$\tau_{av}=\frac{A_1\tau_1^2+A_2\tau_2^2}{A_1\tau_1+A_2\tau_2} \quad (1)$$

The average lifetime of this GO-F system is estimated to be τ_{av} ~ 4.65 ns. The observed lifetime of GO-F is in nanoseconds, suggesting that the synthesized GO-F hybrid material is most suitable for biological applications.

As hypothesized, GO-F hybrid nanosuspensions can be used for biological applications such as bioimaging, cell tracking, and drug delivery, if the inherent toxicity of the material allows it. Therefore, the cytotoxicity of GO-F was evaluated using the MTT viability assay with two different human breast cancer cell lines, MDA-MB-231 and T47D, for the indicated period of time. As shown in Figure 3 (Figure S4), no marked cell death or proliferation defects were observed with cells cultured in GO-F suspensions compared to the untreated control cells, suggesting that GO-F does not pose any considerable toxicity problem to the cells.

To determine whether the GO-F hybrid can be used for cellular imaging, we performed in vitro cellular imaging studies using the human breast cancer cell line T47D. Figure 4a shows fluorescent microscopy images of T47D cells treated with GO-F for 24 h (its biocompatibility is shown in Figure S4; cell viability is consistent with the study on the other cell line MDA-MB-231). The blue fluorescent GO-F is distributed inside the cytoplasm as shown in Figures 4aii, iii, v, and vi. The Figures 4aiv–vi show magnified views of individual T47D cells treated with GO-F. The overlap of fluorescence and phase contrast images clearly shows the cellular localization of GO-F (an individual cell staining is shown in Figure S4 in the Supporting Information; it indicates that the nanoparticles are distributed outside the cell nucleus and inside the cell cytoplasm). Another breast cancer cell line named SUM159PT, which is a metastatic breast cancer cell, was also imaged using the fluorescence of GO-F and is shown in Figure S5 in the Supporting Information.

Nowadays, MRI is widely used to aid the diagnosis of many medical disorders. It is a safe non-invasive technique for medical imaging compared to other techniques such as X-ray computer tomography, where ionizing radiations are used. Moreover, owing to subtle physicochemical differences between organs and tissues, MRI is capable of differentiating tissue type and diseases that may not be detected by other imaging techniques. In order to evaluate GO-F as a potential MRI T2 contrast agent, GO-F was suspended in agarose in graded concentrations and T2 values were measured on a 7T MR scanner with a multi-slice multi-echo (MSME) sequence. The results were fitted into a three-parameter spin–spin relaxation equation using Matlab. The T2 value of 2% agarose phantom was greatly reduced from 111.9 to 33.8 and 61.7 ms when doped with 100 $\mu g\ mL^{-1}$ and 10 $\mu g\ mL^{-1}$ GO-F, respectively. T2-weighted MR images are shown in Figure 4b. To calculate molar relaxivity, we used XPS to determine the elemental percentage of iron in GO-F. On a molar basis, GO-F was 63.42% carbon, 35.64% oxygen, and 0.94% iron. Based on GO-F's iron content, its T2 relaxivity was 297.06 $mM^{-1}\ s^{-1}$. As expected, GO-F did not enhance T1 relaxivity. High contrast even with 100 $\mu g\ mL^{-1}$ (with these amounts no cell death has been observed) indicates that GO-F is a unique material for MRI clinical imaging. In order to find applications of this magnetic GO-F in other fields, such as therapy, thermal conductivity measurements have been conducted and details are provided in the Supporting Information. Enhanced thermal conductivity of GO-F also shows its possibilities in magnetic hyperthermia.

In conclusion, we have demonstrated a 2D hybrid nanostructure-based nanofluid that can be used as a contrast agent in a dual mode imaging process, and that allows one to easily

combine two complementary techniques (T2 MRI and optical fluorescence imaging) in cellular imaging. An interfacial energy transfer mechanism has been identified for the PL of GO-F. The time-resolved spectroscopy measurements reveal a nanosecond decay for hybrid GO-F fluid, indicating its potential applications in biological systems. The hybrid GO-F fluid showed good cell viability with different cancer cell lines. This nanofluid exhibited an enhanced thermal conductivity and the nanoparticles of GO-F were found to penetrate the cell cytoplasm, making it viable for intra-cellular magnetic hyperthermia applications. The surface functionalities in GO provide a good platform for large loading of aromatic drug molecules, thereby avoiding “drug burst” effects associated with bare SPIONs.

Experimental Section

GO-F synthesis

GO was synthesized in water using a modified Hummers’ method as previously reported. [39] Uniformly sized Fe_3O_4 nanoparticles were synthesized within the GO suspension using a chemical co-precipitation technique. $FeSO_4{\cdot}7H_2O$ (1 mL, 0.1 M) and $FeCl_3$ (1 mL, 0.2 M) were placed in a conical flask and mixed well using sonication. 1 mL of this solution was added to 10 mL of the GO suspension and magnetically stirred for half an hour. Ammonia solution was dropped into this mixture with constant stirring until the pH of the solution reached 10 and the Fe_3O_4 nanoparticles started to precipitate within the GO. As soon as the pH reached 10, a 3 M citric acid solution was added dropwise while the solution was heated to 75 °C with constant magnetic stirring for 30 min. This solution was filtered (100 nm Teflon filter paper) and washed several times using distilled water until neutral pH was reached. The resultant filtrate was re-dispersed in distilled water using extensive sonication.

Characterization tools

The structural and morphological analyses of GO-F powder were carried out using HRTEM (JEM 2100F transmission electron microscope), and the Raman study was conducted using a micro-Raman spectroscope (Renishaw, inVia). Room temperature magnetic properties were probed using a VSM. XRD studies were conducted using Cu Kα radiation. FTIR studies on the sample were performed using a Nicolet FTIR microscope, while XPS was carried out using a PHI Quantera X-ray photoelectron microscope. UV-vis spectra were collected using a high resolution UV-vis spectrophotometer (Shimadzu, model no. UV-2450) using quartz cells with a 10 mm path length. PL characterization was conducted using a luminescence spectrometer (NanoLog, Horiba Jobin Yvon) with a xenon lamp as the source of excitation. TRPL was recorded using a time-correlated single photon counting technique with an Edinburgh Instruments spectrometer (model No. FLSP-920) and picosecond laser diode as the source of excitation.

Cytotoxicity and cellular imaging methods

The cells were cultured and maintained in Dulbecco’s Modified Eagle’s Medium (DMEM), high glucose 1X (Invitrogen), containing 4.5 g L^{-1} D-glucose, 4 mM L-glutamine, and 110 mg L^{-1} sodium pyruvate, with 10% fetal bovine serum (FBS), 100 IU mL^{-1} penicillin, and 100 μg mL^{-1} streptomycin. For the cytotoxicity assay, MDA-MB231 and T47D cells (5×10^3 cells per well) were cultured in 96-well plates, overnight. Different concentrations of GO-F (0–100 μg mL^{-1}) in culture media were added to each well in triplicate. After24 h and 48 h of culture with GO-F, cells were washed gently with 200 μL warm, sterile phosphate-buffered saline (PBS), and then 200 μL/well of MTT reagent [3-(4,5-dimethyl-2-thiazolyl)-2,5-diphenytetrazolium bromide (4 mg mL^{-1})] was added. After 4 h of incubation, MTT reagent was removed and 200 μL of dimethyl sulfoxide (DMSO) was added per well and incubated for an additional 5 min at room temperature. The optical

density of solubilized formazan salts was assessed at 570 nm in a Tecan Infinite M200 microplate reader (Männedorf, Switzerland).

For imaging, 1×10^4 cells/well were plated in four-well sterile chamber slides (Nunc, Rochester, NY) with 500 μL culture medium. After overnight culture, 50 μg mL^{-1} GO-F suspension was added to the culture medium and incubated under regular cell culture conditions. After 4 h and 24 h of culture, medium with GO-F was removed from the cells and washed two times with 1 mL 1X PBS. Cells were fixed using 1% paraformaldehyde and mounted with Vectashield antifade mounting media (Vector Laboratories, Burlingame, CA). Cellular imaging was carried out using a Nikon Eclipse 90i microscope equipped with the Cool SnaP HQ2 CCD camera (Photometrics, Tucson, AZ). A Nikon Intensilight C-HGFI lamp was used as the fluorescence light source.

Thermal conductivity measurements on GO-F

The effective thermal conductivities of nanofluids were measured using a thermal properties analyzer (Decagon Devices Inc., Pullman, WA, model KD2 Pro). This device is based on the transient hot-wire technique. Here, a finite-length wire is completely immersed in a finite volume of GO-F. While the wire is heating up, the change in resistance (thus its temperature) is measured as a function of time using a Wheatstone bridge circuit. The thermal conductivity (TC) value is determined from the heating power and the slope of the temperature change with logarithmic time scale. The instrument uses a 1.3 mm diameter by 60 mm long stainless steel probe that is immersed in the nanofluids to obtain the thermal conductivity. The instrument was calibrated using glycerin and measurement was verified up to three decimal places.

T2 MRI measurements

In order to evaluate GO-F as a potential MRI T2 contrast agent, agarose phantoms were made with GO-F. Their T2 values were measured on a 7T MR scanner with a MSME sequence and the results were fitted to a three-parameter spin–spin relaxation equation using Matlab.

Supplementary Material

Refer to Web version on PubMed Central for supplementary material.

Acknowledgments

T.N.N. and P.M.A. gratefully acknowledge financial support from Nanoholdings LLC, Rowayton, CT. B.K.G. thanks the Indo-US Science and Technology Forum (IUSSTF) for financial support. S.V.T., B.X., and P.M.A. acknowledge support from RO1CA12842 and R01CA128428-02S1 from the National Institutes of Health.

References

1. Mahmoudi M, Serpooshan V, Laurent S. Nanoscale. 2011; 3:3007. [PubMed: 21717012]
2. Narayanan TN, Reena Mary AP, Swalih PKA, Sakthi Kumar D, Makarov D, Albrecht M, Puthumana J, Anas A, Anantharaman MR. J Nanosci Nanotechnol. 2011; 11:1958. [PubMed: 21449334]
3. Block S, Glöckl G, Weitschies W, Helm CA. Nano Lett. 2011; 11:3587. [PubMed: 21819124]
4. McCarthy JR, Kelly KA, Sun EY, Weisslender R. Nanomedicine. 2007; 2:153. [PubMed: 17716118]
5. Richard C, Doan B-T, Beloeil J-C, Bessodes M, Tóth E, Scherman D. Nano Lett. 2007; 8:232. [PubMed: 18088153]

6. Zhao Y, Vivero-Escoto JL, Slowing II, Trewyn BG, Lin VSY. Expert Opin Drug Deliv. 2010; 7:1013. [PubMed: 20716017]
7. Hoare T, Santamaria J, Goya GF, Irusta S, Lin D, Lau S, Padera R, Langer R, Kohane DS. Nano Lett. 2009; 9:3651. [PubMed: 19736912]
8. Habib AH, Ondeck CL, Chaudhari P, Bokkstaller MR, McHenry ME. J Appl Phys. 2008; 103:07A307.
9. Zhang H, Pan D, Zou K, He J, Duan X. J Mater Chem. 2009; 19:3069.
10. Zhu M, Diao G. Nanoscale. 2011; 3:2748. [PubMed: 21611651]
11. Levi-Polyachenko NH, Merkel EJ, Jones BT, Carroll DL, Stewart JH. Mol Pharmaceutics. 2009; 6:1092.
12. Sun X, Liu Z, Welsher K, Robinson JT, Goodwin A, Zaric S, Dai H. Nano Res. 2008; 1:203. [PubMed: 20216934]
13. Wang K, Ruan J, Song H, Zhang J, Wo Y, Guo S, Cui D. Nanoscale Res Lett. 2011; 6:2.
14. Gilchrist RK, Medal R, Shorey WD, Hanselman RC, Parrott JC, Taylor CB. Ann Surgery. 1957; 146:596.
15. Frullano L, Meade TJ. J Biol Inorg Chem. 2007; 12:939. [PubMed: 17659368]
16. Mulder WJM, Griffioen AW, Strijkers GJ, Cormode DP, Nicolay K, Fayad ZA. Nanomedicine. 2007; 2:307. [PubMed: 17716176]
17. Mulder WJM, Koole R, Brandwijk RJ, Storn G, Chin PTK, Strijkers GJ, de Mello Donegá C, Nicolay K, Griffioen AW. Nano Lett. 2006; 6:1. [PubMed: 16402777]
18. Gupta BK, Rathee V, Narayanan TN, Thanikaivelan P, Saha A, Govind S, Singh P, Shanker V, Marti AA, Ajayan PM. Small. 2011; 7:1767. [PubMed: 21591255]
19. Jin Y, Jia C, Huang S-W, O'Donnell M, Gao X. Nat Commun. 2010; 1:41. [PubMed: 20975706]
20. Mahmoudi M, Amiri H, Shokrgozar MA, Sasanpour P, Rashidian B, Laurent S, Casula MF, Lascialfari A. Chem Commun. 2011; 47:10404.
21. Mahmoudi M, Serpooshan V. ACS Nano. 201210.1021/nn300042m
22. Kassaee MZ, Motamedi E, Majdi M. Chem Eng J. 2011; 170:540.
23. He F, Fan J, Ma D, Zhang L, Leung C, Chan HL. Carbon. 2010; 48:3139.
24. Shen J, Hu Y, Shi M, Li N, Ma H, Ye M. J Phys Chem C. 2010; 114:1498.
25. Amiri H, Mahmoudi M, Lascilfari A. Nanoscale. 2011; 3:1022. [PubMed: 21152576]
26. Mahmoudi M, Simchi A, Imani M, Hafeli UO. J Phys Chem C. 2009; 113:8124.
27. Renyun Z, Magnus H, Gang L, Hakan O. Carbon. 2011; 49:1126.
28. Reena Mary AP, Narayanan TN, Sunny V, Sakthikumar D, Yoshida Y, Joy P, Anantharaman MR. Nanoscale Res Lett. 2010; 5:1706. [PubMed: 21076702]
29. Mahmoudi M, Serpooshan V. J Phys Chem C. 2011; 115:18275.
30. Mahmoudi M, Lynch I, Ejtehadi MR, Monopoli MP, Baldelli F, Laurent S. Chem Rev. 2011; 111:5610. [PubMed: 21688848]
31. Nel AE, Madler L, Velegol D, Xia T, Hoek EMV, Somasundaran P, Klaessig F, Castranova V, Thompson M. Nat Mater. 2009; 8:543. [PubMed: 19525947]
32. Jin M, Jeong H-K, Yu WJ, Bae DJ, Kang BR, Lee Y. J Phys D: Appl Phys. 2009; 42:135109.
33. Li GH, Wu YC, Zhang LD. Chin Phys. 2001; 10:148.
34. Zhou ZH, Xue JM, Chan HSO, Wang J. J Appl Phys. 2001; 90:4169.
35. Chen W, Zhang J. Scr Mater. 2003; 49:321.
36. Thomas S, Sakthikumar D, Yoshida Y, Anantharaman MR. J Nanoparticle Res. 2008; 10:203.
37. Murakami S, Herren M, Rau D, Morita M. Inorg Chim Acta. 2000; 1014:300.
38. Fujii T, Kodaira K, Kawauchi O, Tanaka N. J Phys Chem B. 1997; 101:10631.
39. Gao W, Majumdar M, Alemany LB, Narayanan TN, Ibarra MA, Pradhan B, Ajayan PM. ACS Appl Mater Interfaces. 2011; 3:1821. [PubMed: 21568266]

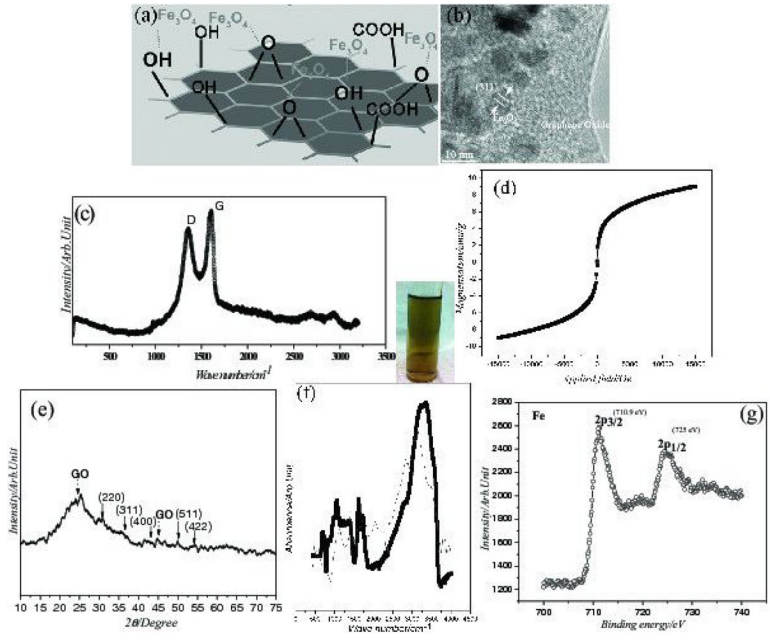

Figure 1.

a) Schematic of the hybrid GO-F. Fe_3O_4 nanoparticles are covalently attached to the graphene plane through oxygen functionalities. b) Transmission electron microscopy (TEM) image of GO-F showing the Fe_3O_4 nanoparticles distributed throughout GO. c) Micro-Raman spectrum. Graphitic order and disorder (G and D) Raman modes are marked. Photograph: GO-F suspension in water. d) Room temperature magnetization curve of GO-F powder. The S-like $M(H)$ loop shows the superparamagnetic nature of the GO-F powder (paramagnetic contribution from the graphite lattice is not subtracted). e) X-ray diffraction (XRD) of GO-F. f) FTIR of GO (dark line) and GO-F (dots) g) Fe 2p X-ray photoelectron spectroscopy (XPS) spectrum of GO-F.

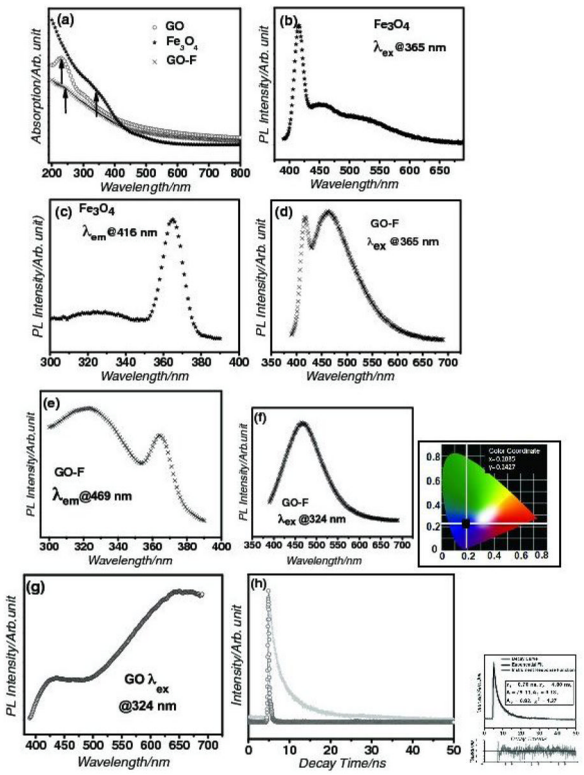

Figure 2.

a) UV-vis absorption spectra of Fe_3O_4, GO, and GO-F fluids. b) Room temperature PL emission spectrum of Fe_3O_4 nanoparticles at 365 nm excitation. c) PL excitation spectrum at 416 nm emission of Fe_3O_4 nanoparticles. d) PL emission spectrum of GO-F nanofluid at 365 nm excitation. e) PL excitation spectrum at 416 nm emission of GO-F nanofluid. Note that an additional interface peak appears after GO forms an interface with Fe_3O_4. f) PL emission spectrum of GO-F nanofluid at 324 nm excitation. g) The color coordinate of the blue emission. h) PL emission spectrum of GO at 324 nm excitation. i) TRPL decay profile of GO-F nanofluid recorded at room temperature while monitoring the emission at 469 nm at an excitation wavelength of 371 nm. j) The lifetime data and the parameter generated by the exponential fitting.

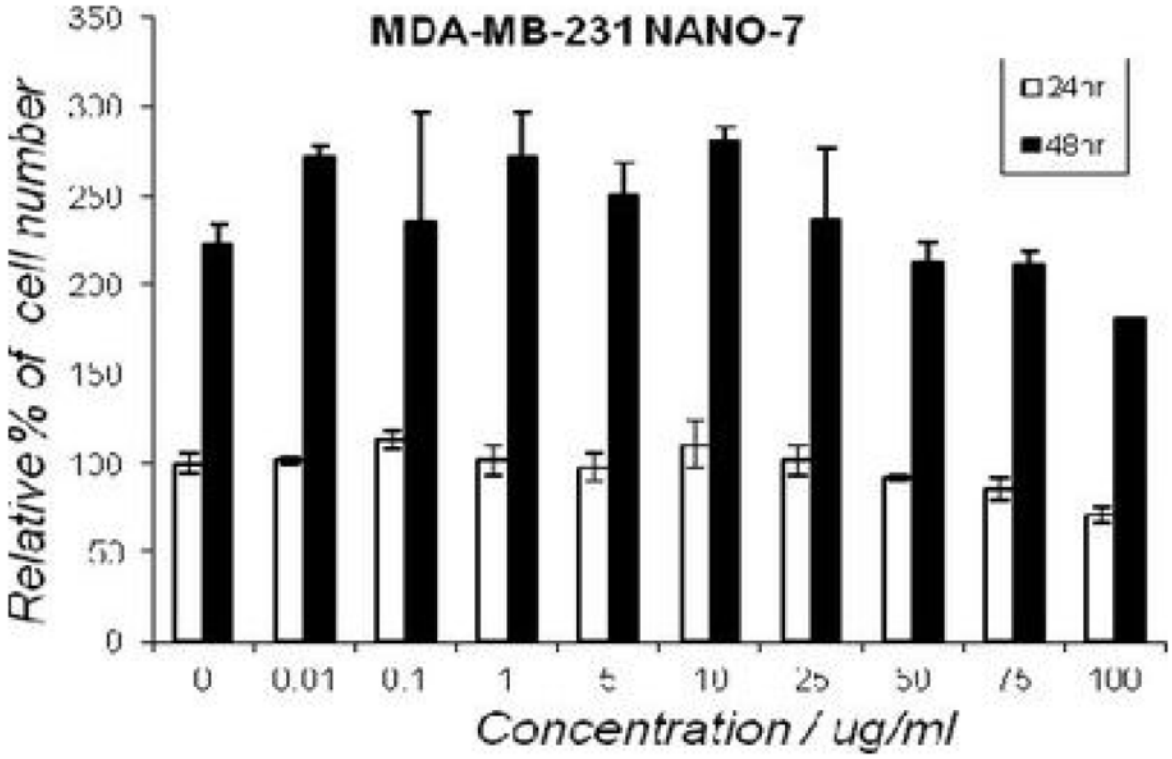

Figure 3.
Cell viability assay with human breast cancer cell lines MDA-MB-231. Cells were treated with different concentrations of GO-F. No significant cytotoxicity was observed with various doses of GO-F treatment.

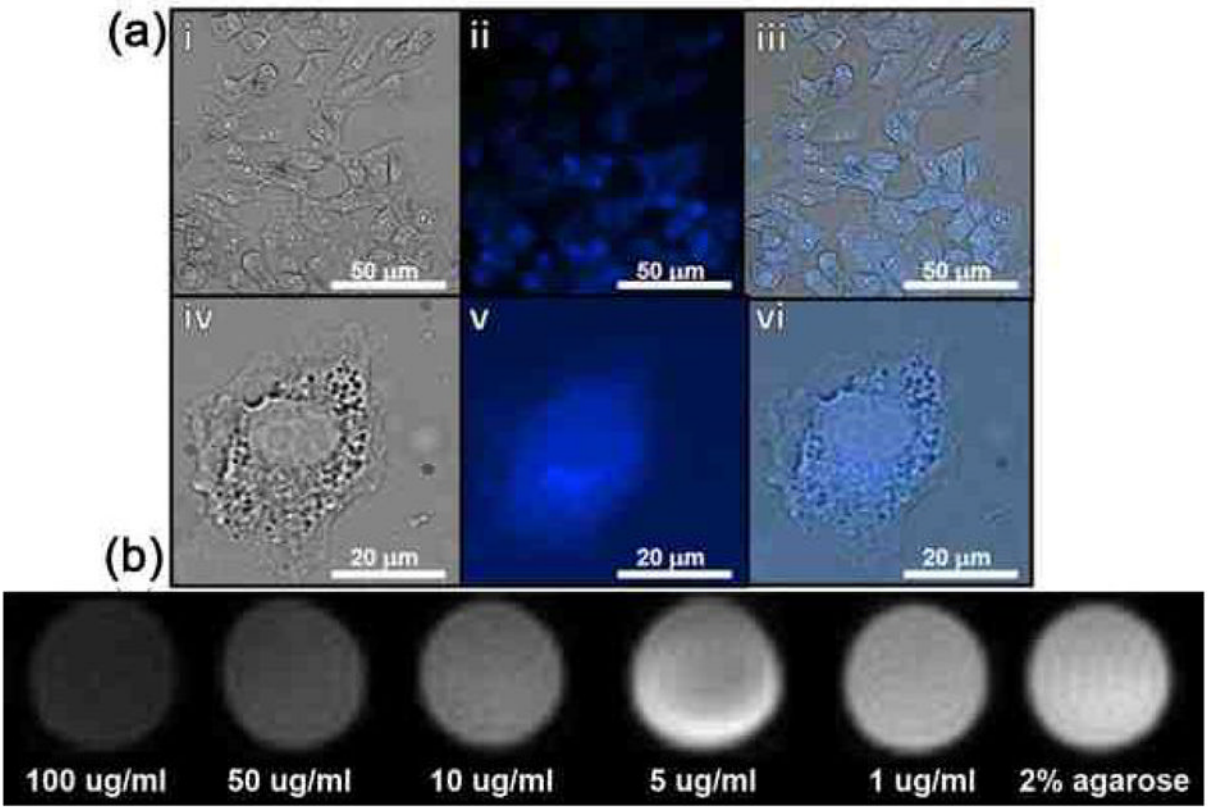

Figure 4.

a) In vitro fluorescence microscopy images of T47D cells treated with GO-F (50 μg mL^{-1}) for 24 h. i–iii) Low magnification images of T47D cells: i) Phase contrast picture, ii) fluorescence images of GO-F, and iii) overlay of images (i) and (ii). iv–vi) High magnification images of an individual T47D cell: iv) phase contrast picture of an individual T47D cell, v) fluorescence image of GO-F, and vi) overlay of images (iv) and (v). The overlay of the phase contrast and fluorescence images clearly demonstrates the localization of GO-F in the cellular cytoplasm, suggesting its suitability for bioimaging. b) T2-weighted MR image showing strong T2 contrast in agarose phantoms. It shows alginate phantoms doped with different concentrations (as shown) of GO-F. The T2-weighted image was acquired in a 7T scanner with multi-slice multi-echo sequence. The T2 relaxivity was 297.06 mM^{-1} s^{-1}.